J. Fluid Mech. (2011), *vol.* 681, *pp.* 241–260. © Cambridge University Press 2011
doi:10.1017/jfm.2011.195

H_2 optimal actuator and sensor placement in the linearised complex Ginzburg–Landau system

KEVIN K. CHEN† AND CLARENCE W. ROWLEY

Department of Mechanical and Aerospace Engineering, Princeton University, Princeton, NJ 08544, USA

(Received 27 July 2010; revised 23 December 2010; accepted 22 April 2011;
first published online 20 June 2011)

The linearised complex Ginzburg–Landau equation is a model for the evolution of small fluid perturbations, such as in a bluff body wake. By implementing actuators and sensors and designing an H_2 optimal controller, we control a supercritical, infinite-domain formulation of this system. We seek the optimal actuator and sensor placement that minimises the H_2 norm of the controlled system, from flow disturbances and sensor noise to a cost on the perturbation and input magnitudes. We formulate the gradient of the H_2 squared norm with respect to the actuator and sensor placements and iterate towards the optimal placement. When stochastic flow disturbances are present everywhere in the spatial domain, it is optimal to place the actuator just upstream of the origin and the sensor just downstream. With pairs of actuators and sensors, it is optimal to place each actuator slightly upstream of each corresponding sensor, and scatter the pairs throughout the spatial domain. When disturbances are only introduced upstream, the optimal placement shifts upstream as well. Global mode and Gramian analyses fail to predict the optimal placement; they produce H_2 norms about five times higher than at the true optimum. The wavemaker region is a better guess for the optimal placement.

Key words: absolute/convective instability, control theory, instability control

1. Introduction

Stability theory has been an active field of fluid mechanics research because of its prevalence in physical phenomena. A common characteristic of stability theory is the simplification of the full Navier–Stokes equations to an amplitude equation of reduced dimension. This is often done out of practicality, since reduced-dimensional models are more tractable and easier to analyse. The Ginzburg–Landau equation is one such model that is often used to study fluid instabilities in spatially developing flows (Huerre & Monkewitz 1990); it has been applied to bluff body wakes, jets and other configurations (see Chomaz, Huerre & Redekopp 1988; Cossu & Chomaz 1997; Lauga & Bewley 2004; Bagheri *et al.* 2009).

The Ginzburg–Landau equation describes the temporal and spatial evolution of velocity perturbations in a given flow configuration. It is a complex partial differential equation first-order in time and second-order in one spatial dimension, the streamwise direction. As such, it serves as a convenient starting point for establishing a flow control model without the complexities of a full two- or three-dimensional Navier–Stokes system. If flow field perturbations are sufficiently small, then the equation's cubic term can be truncated to form a linear partial differential equation.

† Email address for correspondence: kkchen@princeton.edu

https://doi.org/10.1017/jfm.2011.195 Published online by Cambridge University Press

The articles by Bagheri *et al.* (2009) and Lauga & Bewley (2004) employed a flow control framework for the linearised Ginzburg–Landau equation. They modelled the flow dynamics, actuator effect and probe sensing as a standard linear state space. This representation carries the benefit that linear time-invariant (LTI) control theory is a highly developed field of study; results from optimal control, robust control and model reduction are directly applicable. These papers analysed the transient and long-time stability of the Ginzburg–Landau system using a single-input, single-output (SISO) feedback loop—that is, with one actuator manipulating the flow at one point in space, acting on information from one sensor located at another point in space. Bagheri *et al.* emphasised model reduction of the system and linear quadratic Gaussian (LQG) control (which is a specific instance of H_2 optimal control) in the presence of an upstream disturbance. Lauga & Bewley, on the other hand, focused on H_∞-based robust control.

The present study expands on the H_2 optimal control framework by investigating where actuators and sensors should be placed for maximum reduction of the flow perturbation and actuator effort, given an exogenous flow disturbance. The current fluid mechanics literature has few analytically rigorous studies on optimal actuator and sensor placement. Bagheri *et al.* (2009) and Åkervik *et al.* (2007) stated that sensor locations should overlap with unstable global modes, and actuator locations with corresponding adjoint modes; they placed their sensor and actuator at the mode magnitude maxima. These detectability and stabilisability conditions are necessary for the construction of the H_2 optimal control solution (Doyle *et al.* 1989). As will become evident in this paper, however, actuator and sensor placement by modal analysis yields suboptimal control. Although such a placement may be sufficient for preventing large-scale self-sustaining global oscillations, it may be insufficient for applications where transient growth needs to be reduced.

In an early study, Strykowski & Sreenivasan (1990) placed a small secondary cylinder in the wake of a larger primary cylinder and plotted the placements where the secondary cylinder was passively able to suppress vortex shedding for given Reynolds numbers. Giannetti & Luchini (2007) showed that Strykowski & Sreenivasan's placements corresponded with the wavemaker region of the Navier–Stokes operator linearised about the unstable equilibrium wake. Gillies (2001) similarly placed an actuator in the absolutely unstable part of the domain and experimentally showed that his controllers were successful only when the sensors were also in the absolutely unstable domain. These results were consistent with those of Roussopoulos (1993), who experimented with sensor placement in a wind tunnel and a water channel. Lauga & Bewley (2004) placed an actuator and a sensor in the wavemaker region of the Ginzburg–Landau equation. In an earlier study, Lauga & Bewley (2003) employed a linear quadratic regulator with full-state feedback; they tracked the movement of the optimal actuator placement as the supercriticality parameter increased.

Much of the analytically rigorous literature on optimal actuator and sensor placement is related to the vibration control of flexible structures. For instance, Moheimani & Ryall (1999) placed collocated actuator and sensor pairs where they were able to control all important vibration modes. Kondoh, Yatomi & Inoue (1990) employed Powell's method of multidimensional function minimisation to locate H_2 optimal actuator and sensor positions, but reported that the iterative technique became difficult as the number of actuators and sensors increased. Hiramoto, Doki & Obinata (2000) formulated the gradient of the controlled system's H_2 norm with respect to actuator and sensor locations, allowing the use of gradient-based minimisation techniques. The framework developed, however, assumed collocation of the actuator and sensor.

https://doi.org/10.1017/jfm.2011.195 Published online by Cambridge University Press

Vibration control of flexible structures benefits from the fact that the dynamical evolution operator is normal (Hiramoto *et al.* 2000), and eigenfunctions are orthogonal (Halim & Moheimani 2003). On the other hand, the linearised Ginzburg–Landau and Navier–Stokes operators are non-normal, and their global modes do not form an orthogonal basis (Cossu & Chomaz 1997; Chomaz 2005; Bagheri *et al.* 2009). Therefore, methods for optimal placement in the flexible structures literature generally do not apply to fluid systems. Ideally, techniques should analytically or numerically compute optimal placement without iteration. In the absence of such techniques, the Powell's method of Kondoh *et al.* (1990) and the gradient-based minimisation of Hiramoto *et al.* (2000) serve as good starting points for the Ginzburg–Landau system.

In this paper, we seek the actuator and sensor placement that minimises the perturbation magnitude and actuator effort of the Ginzburg–Landau system in an H_2 sense. We investigate cases in which a white noise flow disturbance is present everywhere in the domain or only in the upstream region. The underlying idea is that while H_2 optimal control theory can provide the 'best' controller given an actuator and sensor placement, the 'best' placement should ideally be sought in conjunction. We develop an improved formulation of Hiramoto *et al.*'s H_2 norm gradient. We employ the conjugate gradient method of multidimensional function minimisation for SISO as well as multiple-input, multiple-output (MIMO) control of the Ginzburg–Landau equation. For the SISO cases, we compare the conjugate gradient results to brute force sampling results, where we evaluate the H_2 optimal controller and the corresponding system norm for a large test matrix of actuator and sensor positions. Finally, we discuss the failure of global mode and Gramian analyses to yield the optimal placement, and we suggest that the wavemaker region is a better indicator of the optimal placement.

2. Complex Ginzburg–Landau equation

2.1. *Continuous representation*

A complete discussion of the Ginzburg–Landau equation is too expansive to be given here. For a more comprehensive review, refer to the review article by Bagheri *et al.* (2009).

For a velocity or streamfunction perturbation amplitude given by the real part of $q(x,t)$, the complex Ginzburg–Landau equation is

$$\frac{\partial q}{\partial t} + \nu \frac{\partial q}{\partial x} = \mu(x)\, q + \gamma \frac{\partial^2 q}{\partial x^2} - a\,|q|^2\, q. \tag{2.1}$$

We choose the spatial domain of q to be fully infinite, requiring $q(\pm\infty, t) = 0$ (Cossu & Chomaz 1997; Chomaz 2005). This allows perturbations to grow and decay throughout the entire streamwise dimension. With this choice of a domain, we typically assume that the physical feature of interest is at $x = 0$. The complex advection speed is $\nu = U + 2\mathrm{i}c_u$, the complex diffusion parameter is $\gamma = 1 + \mathrm{i}c_d$ and the amplification factor is $\mu(x) = \mu_0 - c_u^2 + \mu_2 x^2/2$ (Bagheri *et al.* 2009). The mean advection velocity is given by $U > 0$, and c_u, μ_0 and a are also positive quantities; μ_2 and c_d are negative (Cossu & Chomaz 1997; Chomaz 2005). Numerical values of these parameters are determined empirically (Williamson 1996; Roussopoulos & Monkewitz 1996).

The nonlinear term $-a|q|^2q$ causes a Hopf bifurcation expected in many geometrical configurations (e.g. Sreenivasan, Strykowski & Olinger 1987). In a linear analysis, the flow is assumed to be near the equilibrium state $q = 0$; thus, $-a|q|^2q \approx 0$. The resulting

https://doi.org/10.1017/jfm.2011.195 Published online by Cambridge University Press

linear equation is

$$\dot{q} = \mathrm{L}q, \tag{2.2a}$$

where

$$\mathrm{L} \triangleq -\nu\frac{\partial}{\partial x} + \mu(x) + \gamma\frac{\partial^2}{\partial x^2} \tag{2.2b}$$

defines the linear operator L. From this point forward, we will always truncate the cubic term and refer only to the linear system.

We now comment on the stability properties of the linearised Ginzburg–Landau system, drawing from results found in Bagheri *et al.* (2009) and Cossu & Chomaz (1997). In the parabolic construction $\mu(x) = \mu_0 - c_u^2 + \mu_2 x^2/2$, the region of amplification is the part of the domain where $\mu(x) > 0$; this corresponds to $-\sqrt{-2(\mu_0 - c_u^2)/\mu_2} < x < \sqrt{-2(\mu_0 - c_u^2)/\mu_2}$. The quantity $\mu_0 - c_u^2$ is the greatest amplification factor present in the physical domain, occurring at $x = 0$; μ_0 is derived from the Reynolds number. If $\mu_0 - c_u^2 < 0$, then the flow is stable everywhere, and all perturbations decay with time. Otherwise, at least some part of the domain exhibits amplification (convective or absolute instability), and c_u is the most unstable spatial wavenumber.

In the analysis of parallel flows (where μ is constant), we construct a transitional value $\mu_t = U_{max}^2/(4|\gamma|^2)$, with $U_{max} = U + 2c_d c_u$ the group velocity. When $0 < \mu < \mu_t$, the domain is convectively unstable. The response $G(x,t)$ to an impulse $\delta(x)\delta(t)$ blows up along $x = kt$ for at least one value of k as $t \to \infty$, but $\lim_{t\to\infty} G(0,t) = 0$. When $\mu_t < \mu$, the domain is absolutely unstable, and $\lim_{t\to\infty} G(0,t) = \infty$ (Schmid & Henningson 2000).

Returning to the non-parallel case, where μ is parabolic in space, we also define a critical value $\mu_c = \mu_t + |h|\cos((\mathrm{Arg}\ \gamma)/2)/2$, where $h = \sqrt{-2\mu_2\gamma}$. Global stability is lost if and only if $\mu_0 > \mu_c$; this is a direct result of the eigendecomposition of L. Eigenvalues, eigenmodes and adjoint modes are given, respectively, by

$$\lambda_n = \mu_0 - c_u^2 - \frac{\nu^2}{4\gamma} - \left(n + \frac{1}{2}\right)h, \tag{2.3a}$$

$$\phi_n(x) = \exp\left(\frac{1}{2}\left(\frac{\nu x}{\gamma} - \chi^2 x^2\right)\right) H_n(\chi x), \tag{2.3b}$$

$$\psi_n(x) = \exp\left(-\frac{\bar{\nu} x}{\bar{\gamma}}\right)\bar{\phi}_n(x), \tag{2.3c}$$

where $n = 0, 1, \ldots,$ $\chi = (-\mu_2/(2\gamma))^{1/4}$, H_n is the nth Hermite polynomial and $\overline{(\cdot)}$ indicates a complex conjugate. If $\mathrm{Re}[\lambda_0] > 0$, then the system must be globally unstable. Otherwise, it is globally stable and perturbations eventually decay with time, but transient perturbation growth may still exist.

Finally, we note briefly that μ_2 denotes how non-parallel the flow is; it is partly responsible for determining the size of the amplification region. In addition, c_d is a dispersion parameter, but we will not discuss it further. See Bagheri *et al.* (2009) for additional details.

The Ginzburg–Landau parameters chosen for this study are drawn from Bagheri *et al.* (2009) and are shown in table 1. This study primarily investigates a supercritical, globally unstable system, with $\mu_0 = 1.03\mu_c$. When we consider subcritical, globally stable systems, however, we use $\mu_0 = 0.96\mu_c$. We always assume supercriticality unless stated otherwise.

https://doi.org/10.1017/jfm.2011.195 Published online by Cambridge University Press

Variable	Description	Value
U	Mean advection velocity	2.0
c_u	Most unstable wavenumber	0.2
c_d	Dispersion parameter	-1.0
μ_0	Overall amplification	0.41 (0.38)
μ_2	Degree of non-parallelism	-0.01
μ_t	Transitional μ	0.32
μ_c	Critical μ	0.40
a	Nonlinearity	not used
x_1, x_N	Extent of discretised domain	-56.06, 56.06
$\pm\sqrt{-2(\mu_0 - c_u^2)/\mu_2}$	Extent of amplification region	± 8.60 (± 8.25)
x_d	Upstream disturbance location	-11.0
σ	Gaussian width	0.4

TABLE 1. Ginzburg–Landau parameters. Subcritical parameters are shown in parentheses.

2.2. *Discrete representation*

To model the Ginzburg–Landau equation as a LTI state space, we spatially discretise the physical domain. We create a domain discretisation and a pseudospectral formulation of $\partial/\partial x$ and $\partial^2/\partial x^2$ using weighted Hermite polynomials, as in Bagheri *et al.* (2009). We draw the discretisation and associated differentiation operators from Weideman & Reddy (2000). The physical domain is represented using $N = 100$ grid points, and these points $\{x_1, x_2, \ldots, x_N\}$ are the roots of $H_N(\mathrm{Re}[\chi]\, x)$. With this choice of N, the discretised domain stretches from $x_1 = -56.06$ to $x_N = 56.06$. For the globally unstable system studied, the region of amplification is $-8.60 < x < 8.60$. We choose $N = 100$ because it achieves sufficient accuracy while maintaining problem tractability. To check for convergence of results in N, we test systems with one actuator and one sensor, and with two actuators and two sensors. In both cases, we introduce flow disturbances across the entire spatial domain (see § 3.1 for details). Increasing N from 100 to 200 changes the computed optimal actuator and sensor placement by less than 1.0% of the amplification region's length.

Using this discretisation scheme, we construct the state vector $\boldsymbol{q} = \begin{bmatrix} q_1 & \cdots & q_N \end{bmatrix}^{\mathrm{T}}$, where $q_j = q(x_j)$ for $j = 1, 2, \ldots, N$. Let $\boldsymbol{D}$ be the Hermite pseudospectral derivative matrix and $\boldsymbol{\Delta}$ be the second derivative matrix. Also, let $\boldsymbol{\mu}$ be $\mu(x)$ discretised in the same way as $\boldsymbol{q}$. Then the discrete representation of the linearised Ginzburg–Landau equation is

$$\dot{\boldsymbol{q}} = \boldsymbol{A}\boldsymbol{q}, \tag{2.4a}$$

where

$$\boldsymbol{A} \triangleq -\nu\boldsymbol{D} + \mathrm{diag}(\boldsymbol{\mu}) + \gamma\boldsymbol{\Delta} \tag{2.4b}$$

is the discrete linearised Ginzburg–Landau operator.

3. H_2 optimal control and placement

In this section, we apply techniques developed in the control theory community, and we use these methods to develop a gradient-based formulation for optimising the actuator and sensor placement. The review article by Kim & Bewley (2007) provides a quick introduction to optimal control theory and its application to fluid mechanics. A complete reference can be found in Skogestad & Postlethwaite (2005). The seminal

https://doi.org/10.1017/jfm.2011.195 Published online by Cambridge University Press

paper by Doyle *et al.* (1989) establishes the H_2 optimal control theory used in this section. Finally, Schmid (2007) reviews important concepts from linear dynamics, such as transfer functions and stochastic dynamics, that we employ.

3.1. *State space setup*

Let us return momentarily to the continuous-space linearised Ginzburg–Landau equation. Instead of implementing a particular type of flow actuator or sensing probe, we apply generic actuation and sensing drawn from the standard state space setup. This way, we can easily take advantage of available LTI tools. We also insert a white noise disturbance d, which may be present everywhere in the spatial domain or centred in the upstream domain. Assume a small sensor white noise n. For a single actuator located at $x = x_a$ and a single sensor at $x = x_s$, the state space is

$$\frac{\partial q}{\partial t}(x,t) = \mathrm{L}q(x,t) + \exp\left(-\frac{(x-x_a)^2}{2\sigma^2}\right) u(t) + d(x,t), \tag{3.1a}$$

$$y(t) = \left\langle q(x,t), \exp\left(-\frac{(x-x_s)^2}{2\sigma^2}\right)\right\rangle + n(t), \tag{3.1b}$$

where $\langle f_1, f_2\rangle \triangleq \int_{-\infty}^{\infty} \bar{f}_2 f_1 \,\mathrm{d}x$ is an inner product. The state q, input signal u, output signal y, disturbance d, and noise n are all complex, and we choose $\sigma = 0.4$.

In discretised form, with $\boldsymbol{A}$ given by (2.4*b*) and all other variables explained below, we recover the standard state space

$$\dot{\boldsymbol{q}} = \boldsymbol{A}\boldsymbol{q} + \boldsymbol{B}_2\boldsymbol{u} + \boldsymbol{W}^{1/2}\boldsymbol{d}, \tag{3.2a}$$

$$\boldsymbol{y} = \boldsymbol{C}_2\boldsymbol{q} + \boldsymbol{V}^{1/2}\boldsymbol{n}. \tag{3.2b}$$

In SISO control, $\boldsymbol{u}$ and $\boldsymbol{y}$ are complex scalars and $\boldsymbol{B}_2$ is an N-by-1 vector discretising $\exp(-(x-x_a)^2/(2\sigma^2))$. For discretised sensing, note that a weighting matrix must be used to carry out the integration implied by (3.1*b*). Let

$$\boldsymbol{M} = \tfrac{1}{2}\mathrm{diag}\left(\left[x_2 - x_1, x_3 - x_1, \cdots, x_{i+1} - x_{i-1}, \cdots, x_m - x_{m-2}, x_m - x_{m-1}\right]\right) \tag{3.3}$$

be the weighting matrix corresponding to the trapezoidal integration operator, and let $\boldsymbol{s}$ be the n-by-1 discretisation of $\exp(-(x-x_s)^2/(2\sigma^2))$. Then the inner product in (3.1*b*) transforms to $\langle \boldsymbol{q}, \boldsymbol{s}\rangle$, where $\langle \boldsymbol{v}_1, \boldsymbol{v}_2\rangle = \boldsymbol{v}_2^*\boldsymbol{M}\boldsymbol{v}_1$ is the discrete inner product and $(\cdot)^*$ indicates a conjugate transpose. This yields $\boldsymbol{C}_2 = \boldsymbol{s}^{\mathrm{T}}\boldsymbol{M}$. In the case of MIMO control, suppose that there exist m_a actuators and m_s sensors. Let $\boldsymbol{b}^j$ be the discretisation of the jth actuator, and $\boldsymbol{s}^k$ the kth sensor. Then $\boldsymbol{B}_2 = [\boldsymbol{b}^1 \cdots \boldsymbol{b}^{m_a}]$, and $\boldsymbol{C}_2 = [\boldsymbol{s}^1 \cdots \boldsymbol{s}^{m_s}]^{\mathrm{T}}\boldsymbol{M}$.

The disturbance and sensor noise are complex white noise stochastic processes. In the case of a disturbance pervading the entire domain, $\boldsymbol{d}$ is an N-by-1 complex white noise signal with covariance $E(\boldsymbol{d}\boldsymbol{d}^*) = \boldsymbol{I}$ (with E the expected value), and we choose $\boldsymbol{W}^{1/2} = \boldsymbol{I}$. If the disturbance is upstream, then $\boldsymbol{d}$ is a complex white noise scalar with unit covariance, and $\boldsymbol{W}^{1/2}$ is the N-by-1 vector discretisation of $\exp(-(x-x_d)^2/(2\sigma^2))$; x_d is fixed at -11.0. We do not wish to place any particular focus on sensor noise in this study, but the noise must be present for the LQG formulation to be well posed. Therefore, $\boldsymbol{n}$ is an m_s-by-1 complex white noise signal with covariance $E(\boldsymbol{n}\boldsymbol{n}^*) = \boldsymbol{I}$, and we choose $\boldsymbol{V}^{1/2} = 2 \times 10^{-4}\boldsymbol{I}$ so that the sensor noise is present but minimal. It will be apparent later that the LQG controller remains well behaved for this small choice of $\boldsymbol{V}^{1/2}$.

3.2. *Linear quadratic Gaussian framework*

Having set up the governing dynamics and input/output relations in (3.1) and (3.2), we now design a controller that determines the control signal $u(t)$ from the sensor

https://doi.org/10.1017/jfm.2011.195 Published online by Cambridge University Press

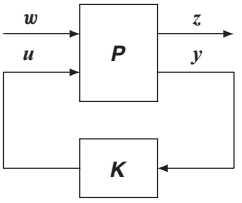


FIGURE 1. General control problem formulation $\boldsymbol{G}$.

output $y(t)$. In particular, we seek the relation from y to u that minimises the perturbation magnitude $\int_{-\infty}^{\infty} |q(x,t)|^2 \,\mathrm{d}x$. This minimisation is the ultimate goal of Ginzburg–Landau control. Realistically, however, we must also keep the input size $|u(t)|^2$ within bounds; a very large input size may be non-physical. Therefore, we establish a cost function

$$J = \beta^2 \int_{-\infty}^{\infty} |q\,(x,t)|^2 \,\mathrm{d}x + |u\,(t)|^2 \tag{3.4}$$

to minimise using the right choice of a controller. The positive scalar β controls the balance between maintaining a small perturbation size and maintaining a small input size. In this study, we choose $\beta = 7$. We discuss different choices of β in § 4.3.

In discrete space, the cost function takes the form $J = \boldsymbol{q}^* \boldsymbol{Q} \boldsymbol{q} + \boldsymbol{u}^* \boldsymbol{R} \boldsymbol{u}$, where $\boldsymbol{Q}$ and $\boldsymbol{R}$ are user-specified penalties on the state and inputs sizes. To be consistent with (3.4), we use $\boldsymbol{Q} = \beta^2 \boldsymbol{M}$ and $\boldsymbol{R} = \boldsymbol{I}$. In vector form, the cost on the perturbation and input sizes are given by $\boldsymbol{J}_1 = \boldsymbol{Q}^{1/2} \boldsymbol{q}$ and $\boldsymbol{J}_2 = \boldsymbol{R}^{1/2} \boldsymbol{u}$, where the matrix square root $\boldsymbol{Z}^{1/2}$ satisfies $(\boldsymbol{Z}^{1/2})^* \boldsymbol{Z}^{1/2} = \boldsymbol{Z}$. Since the disturbance $\boldsymbol{d}$ and sensor noise $\boldsymbol{n}$ are exogenous inputs, minimising J is equivalent to minimising the gain from $\boldsymbol{d}$ and $\boldsymbol{n}$ to the cost vectors $\boldsymbol{J}_1$ and $\boldsymbol{J}_2$.

To establish the relation from $\boldsymbol{d}$ and $\boldsymbol{n}$ to $\boldsymbol{J}_1$ and $\boldsymbol{J}_2$, we first incorporate the cost vectors into the state space in (3.2) to yield

$$\boldsymbol{P}: \begin{bmatrix} \dot{\boldsymbol{q}} \\ \boldsymbol{z} \\ \boldsymbol{y} \end{bmatrix} = \begin{bmatrix} \boldsymbol{A} & \boldsymbol{B}_1 & \boldsymbol{B}_2 \\ \boldsymbol{C}_1 & 0 & \boldsymbol{D}_{12} \\ \boldsymbol{C}_2 & \boldsymbol{D}_{21} & 0 \end{bmatrix} \begin{bmatrix} \boldsymbol{q} \\ \boldsymbol{w} \\ \boldsymbol{u} \end{bmatrix}, \tag{3.5a}$$

where

$$\boldsymbol{z} = \begin{bmatrix} \boldsymbol{J}_1 \\ \boldsymbol{J}_2 \end{bmatrix}, \quad \boldsymbol{w} = \begin{bmatrix} \boldsymbol{d} \\ \boldsymbol{n} \end{bmatrix} \tag{3.5b,c}$$

and

$$\boldsymbol{B}_1 = \begin{bmatrix} \boldsymbol{W}^{1/2} & 0 \end{bmatrix}, \quad \boldsymbol{C}_1 = \begin{bmatrix} \boldsymbol{Q}^{1/2} \\ 0 \end{bmatrix}, \quad \boldsymbol{D}_{12} = \begin{bmatrix} 0 \\ \boldsymbol{R}^{1/2} \end{bmatrix}, \quad \boldsymbol{D}_{21} = \begin{bmatrix} 0 & \boldsymbol{V}^{1/2} \end{bmatrix}. \tag{3.5d–g}$$

Equation (3.5a) is called the 'plant' or simply $\boldsymbol{P}$. Figure 1 is a pictorial representation of the control problem. The controller $\boldsymbol{K}$ determines the input signal $\boldsymbol{u}$ based on the sensor output $\boldsymbol{y}$. The external input to the system is the flow disturbance and sensor noise in $\boldsymbol{w}$, and the system output is the cost $\boldsymbol{z}$ to be minimised.

In the construction of the general LTI controller, we choose matrices $\boldsymbol{K_A}$, $\boldsymbol{K_B}$, $\boldsymbol{K_C}$ and $\boldsymbol{K_D}$ such that

$$\boldsymbol{K}: \begin{bmatrix} \dot{\hat{\boldsymbol{q}}} \\ \boldsymbol{u} \end{bmatrix} = \begin{bmatrix} \boldsymbol{K_A} & \boldsymbol{K_B} \\ \boldsymbol{K_C} & \boldsymbol{K_D} \end{bmatrix} \begin{bmatrix} \hat{\boldsymbol{q}} \\ \boldsymbol{y} \end{bmatrix} \tag{3.6}$$

https://doi.org/10.1017/jfm.2011.195 Published online by Cambridge University Press

determines the actuation signal $\boldsymbol{u}$ based on the output signal $\boldsymbol{y}$. The variable $\hat{\boldsymbol{q}}$ is the state of the controller and is typically an estimate of the plant state $\boldsymbol{q}$. The LQG controller is the LTI controller that minimises the H_2 norm of the transfer function from $\boldsymbol{d}$ and $\boldsymbol{n}$ to $\boldsymbol{J}_1$ and $\boldsymbol{J}_2$. Suppose that $\boldsymbol{G}(s)$ is that matrix transfer function. In other words, for $s \in \mathbb{C}$ and disturbance and sensor noise inputs of the form $\exp(st)$,

$$\begin{bmatrix} \boldsymbol{J}_1 \\ \boldsymbol{J}_2 \end{bmatrix} = \boldsymbol{G}(s) \begin{bmatrix} \boldsymbol{d} \\ \boldsymbol{n} \end{bmatrix} \tag{3.7}$$

dictates the gain and phase from $\boldsymbol{d}$ and $\boldsymbol{n}$ to $\boldsymbol{J}_1$ and $\boldsymbol{J}_2$. Then the H_2 norm is defined as

$$\gamma_2 \triangleq \|\boldsymbol{G}\|_2 \triangleq \sqrt{\frac{1}{2\pi} \int_{-\infty}^{\infty} \operatorname{tr}\left(\boldsymbol{G}^*(\mathrm{i}\omega)\, \boldsymbol{G}(\mathrm{i}\omega)\right) \mathrm{d}\omega} \tag{3.8}$$

and is an average (instead of a worst-case) measure of the gain provided by $\boldsymbol{G}$. Thus, given exogenous inputs, minimising the perturbation magnitude and actuator effort is equivalent to minimising $\|\boldsymbol{G}\|_2$. We implement the LQG controller so that $\|\boldsymbol{G}\|_2$ is automatically minimised.

To construct the LQG controller, solve the continuous algebraic Riccati equations

$$\boldsymbol{A}^*\boldsymbol{X} + \boldsymbol{X}\boldsymbol{A} - \boldsymbol{X}\boldsymbol{B}_2\boldsymbol{R}^{-1}\boldsymbol{B}_2^*\boldsymbol{X} + \boldsymbol{C}_1^*\boldsymbol{C}_1 = 0 \tag{3.9a}$$

$$\boldsymbol{A}\boldsymbol{Y} + \boldsymbol{Y}\boldsymbol{A}^* - \boldsymbol{Y}\boldsymbol{C}_2^*\boldsymbol{V}^{-1}\boldsymbol{C}_2\boldsymbol{Y} + \boldsymbol{B}_1\boldsymbol{B}_1^* = 0 \tag{3.9b}$$

for $\boldsymbol{X}$ and $\boldsymbol{Y}$, and set $\boldsymbol{F} = \boldsymbol{R}^{-1}\boldsymbol{B}_2^*\boldsymbol{X}$ and $\boldsymbol{L} = \boldsymbol{Y}\boldsymbol{C}_2^*\boldsymbol{V}^{-1}$. The LQG controller is then given by

$$\boldsymbol{K}: \begin{bmatrix} \dot{\hat{\boldsymbol{q}}} \\ \boldsymbol{u} \end{bmatrix} = \begin{bmatrix} \boldsymbol{A} - \boldsymbol{B}_2\boldsymbol{F} - \boldsymbol{L}\boldsymbol{C}_2 & \boldsymbol{L} \\ -\boldsymbol{F} & 0 \end{bmatrix} \begin{bmatrix} \hat{\boldsymbol{q}} \\ \boldsymbol{y} \end{bmatrix}. \tag{3.10}$$

The plant (3.5a) and LQG controller (3.10) can be combined to form a single system, known as the linear fractional transformation (LFT) of $\boldsymbol{G}$ and $\boldsymbol{K}$. One representation of the LFT is

$$\begin{bmatrix} \dot{\boldsymbol{q}} \\ \dot{\hat{\boldsymbol{q}}} \\ \boldsymbol{z} \end{bmatrix} = \begin{bmatrix} \boldsymbol{A} & -\boldsymbol{B}_2\boldsymbol{F} & \boldsymbol{B}_1 \\ \boldsymbol{L}\boldsymbol{C}_2 & \boldsymbol{A} - \boldsymbol{B}_2\boldsymbol{F} - \boldsymbol{L}\boldsymbol{C}_2 & \boldsymbol{L}\boldsymbol{D}_{21} \\ \boldsymbol{C}_1 & -\boldsymbol{D}_{12}\boldsymbol{F} & 0 \end{bmatrix} \begin{bmatrix} \boldsymbol{q} \\ \hat{\boldsymbol{q}} \\ \boldsymbol{w} \end{bmatrix}. \tag{3.11}$$

(Often, the LFT is expressed using an error $\boldsymbol{e} = \hat{\boldsymbol{q}} - \boldsymbol{q}$ instead of directly using the state estimate $\hat{\boldsymbol{q}}$.) Denote the upper-left two-by-two matrix block by $\boldsymbol{Z}_{\boldsymbol{A}}$, the upper-right two-by-one block by $\boldsymbol{Z}_{\boldsymbol{B}}$, and the lower-left one-by-two block by $\boldsymbol{Z}_{\boldsymbol{C}}$. If we compute Gramians $\boldsymbol{W}_c$ and $\boldsymbol{W}_o$ by the Lyapunov equations

$$\boldsymbol{Z}_{\boldsymbol{A}}\boldsymbol{W}_c + \boldsymbol{W}_c\boldsymbol{Z}_{\boldsymbol{A}}^* + \boldsymbol{Z}_{\boldsymbol{B}}\boldsymbol{Z}_{\boldsymbol{B}}^* = 0 \tag{3.12a}$$

$$\boldsymbol{Z}_{\boldsymbol{A}}^*\boldsymbol{W}_o + \boldsymbol{W}_o\boldsymbol{Z}_{\boldsymbol{A}} + \boldsymbol{Z}_{\boldsymbol{C}}^*\boldsymbol{Z}_{\boldsymbol{C}} = 0, \tag{3.12b}$$

then the LQG-controlled system's H_2 squared norm is

$$\Gamma_2 \triangleq \|\boldsymbol{G}\|_2^2 = \operatorname{tr}\left(\boldsymbol{Z}_{\boldsymbol{C}}\boldsymbol{W}_c\boldsymbol{Z}_{\boldsymbol{C}}^*\right) \tag{3.13a}$$

$$= \operatorname{tr}\left(\boldsymbol{Z}_{\boldsymbol{B}}^*\boldsymbol{W}_o\boldsymbol{Z}_{\boldsymbol{B}}\right). \tag{3.13b}$$

The above formulations, however, require solutions of $2N$-by-$2N$ matrix equations. A simpler N-by-N formulation is given by

$$\Gamma_2 = \operatorname{tr}\left(\boldsymbol{C}_1\boldsymbol{Y}\boldsymbol{C}_1^*\right) + \operatorname{tr}\left(\boldsymbol{V}^{-1}\boldsymbol{C}_2\boldsymbol{Y}\boldsymbol{X}\boldsymbol{Y}\boldsymbol{C}_2^*\right) \tag{3.14a}$$

$$= \operatorname{tr}\left(\boldsymbol{B}_1^*\boldsymbol{X}\boldsymbol{B}_1\right) + \operatorname{tr}\left(\boldsymbol{R}^{-1}\boldsymbol{B}_2^*\boldsymbol{X}\boldsymbol{Y}\boldsymbol{X}\boldsymbol{B}_2\right). \tag{3.14b}$$

https://doi.org/10.1017/jfm.2011.195 Published online by Cambridge University Press

3.3. *Perturbation technique for optimal placement*

Suppose that a choice of $\boldsymbol{B}_2$ and $\boldsymbol{C}_2$ is H_2 optimal. That is, the choice of $\boldsymbol{B}_2$ and $\boldsymbol{C}_2$ provides the best-performing H_2 optimal controller, given matrix constraints described in § 3.1. It is necessary, but not sufficient, for an appropriately constrained perturbation $\boldsymbol{\delta B}_2 \neq 0$ to produce $\delta\Gamma_2 = 0$; similarly, $\boldsymbol{\delta C}_2 \neq 0$ must produce $\delta\Gamma_2 = 0$. The constraint on $\boldsymbol{\delta B}_2$ is that it must equal the change in $\boldsymbol{B}_2$ when an actuator position moves from x_a to $x_a + \delta x_a$, for a small δx_a. If there is multiple actuation, then $\boldsymbol{\delta B}_2$ can be a perturbation along any one of the actuator positions. The constraint on $\boldsymbol{\delta C}_2$ is completely analogous, except that it is necessary to pay careful attention to the discretised integration operator $\boldsymbol{M}$.

If the actuator location is perturbed from $\boldsymbol{B}_2$ to $\boldsymbol{B}_2 + \boldsymbol{\delta B}_2$, then we can define $\boldsymbol{\delta X}$ such that (3.9*a*) produces a perturbed solution $\boldsymbol{X} + \boldsymbol{\delta X}$. The exact representation is

$$\boldsymbol{A}^*(\boldsymbol{X}+\boldsymbol{\delta X}) + (\boldsymbol{X}+\boldsymbol{\delta X})\boldsymbol{A} - (\boldsymbol{X}+\boldsymbol{\delta X})(\boldsymbol{B}_2+\boldsymbol{\delta B}_2)\boldsymbol{R}^{-1}(\boldsymbol{B}_2+\boldsymbol{\delta B}_2)^*(\boldsymbol{X}+\boldsymbol{\delta X}) + \boldsymbol{C}_1^*\boldsymbol{C}_1 = 0. \quad (3.15)$$

The $O(\delta^0)$ component returns (3.9*a*), as expected. The $O(\delta^1)$ component is

$$(\boldsymbol{A}-\boldsymbol{B}_2\boldsymbol{R}^{-1}\boldsymbol{B}_2^*\boldsymbol{X})^*\boldsymbol{\delta X} + \boldsymbol{\delta X}\left(\boldsymbol{A}-\boldsymbol{B}_2\boldsymbol{R}^{-1}\boldsymbol{B}_2^*\boldsymbol{X}\right) - \boldsymbol{X}\left(\boldsymbol{\delta B}_2\boldsymbol{R}^{-1}\boldsymbol{B}_2^* + \boldsymbol{B}_2\boldsymbol{R}^{-1}\boldsymbol{\delta B}_2^*\right)\boldsymbol{X} = 0, \quad (3.16)$$

which is a Lyapunov equation for $\boldsymbol{\delta X}$. The perturbation in $\boldsymbol{X}$ then produces $\delta\Gamma_2 = \mathrm{tr}(\boldsymbol{V}^{-1}\boldsymbol{C}_2\boldsymbol{Y}\boldsymbol{\delta X}\,\boldsymbol{Y}\boldsymbol{C}_2^*)$ from (3.14*a*). At the optimal actuator location,

$$\delta\Gamma_2 = \mathrm{tr}\left(\boldsymbol{V}^{-1}\boldsymbol{C}_2\boldsymbol{Y}\boldsymbol{\delta X}\,\boldsymbol{Y}\boldsymbol{C}_2^*\right) = 0. \quad (3.17)$$

In summary, given an appropriately constrained $\boldsymbol{B}_2$ and $\delta\boldsymbol{B}_2$, the H_2 optimal $\boldsymbol{B}_2$ is one that produces $\mathrm{tr}\,(\boldsymbol{V}^{-1}\boldsymbol{C}_2\boldsymbol{Y}\boldsymbol{\delta X}\,\boldsymbol{Y}\boldsymbol{C}_2^*) = 0$, where $\boldsymbol{\delta X}$ is the solution to (3.16) and $\boldsymbol{X}$ is the solution to (3.9*a*). For this choice of $\boldsymbol{B}_2$, the actuator position and the controller are simultaneously optimised to minimise the magnitude of flow perturbations and actuator input. Additional steps are required, however, to ensure that the $\boldsymbol{B}_2$ satisfying $\delta\Gamma_2 = 0$ actually minimises Γ_2, instead of yielding a maximum or saddle point.

The procedure for finding the optimal sensor location is similar to the previously described steps. For an appropriate choice of $\boldsymbol{C}_2$ and $\boldsymbol{\delta C}_2$, the optimal $\boldsymbol{C}_2$ is the one that first yields $\boldsymbol{Y}$ by (3.9*b*), then yields $\boldsymbol{\delta Y}$ by the Lyapunov equation

$$\left(\boldsymbol{A}-\boldsymbol{Y}\boldsymbol{C}_2^*\boldsymbol{V}^{-1}\boldsymbol{C}_2\right)\boldsymbol{\delta Y} + \boldsymbol{\delta Y}\left(\boldsymbol{A}-\boldsymbol{Y}\boldsymbol{C}_2^*\boldsymbol{V}^{-1}\boldsymbol{C}_2\right)^* - \boldsymbol{Y}\left(\boldsymbol{\delta C}_2^*\boldsymbol{V}^{-1}\boldsymbol{C}_2 + \boldsymbol{C}_2^*\boldsymbol{V}^{-1}\boldsymbol{\delta C}_2\right)\boldsymbol{Y} = 0, \quad (3.18)$$

and finally satisfies

$$\delta\Gamma_2 = \mathrm{tr}\left(\boldsymbol{R}^{-1}\boldsymbol{B}_2^*\boldsymbol{X}\,\boldsymbol{\delta Y}\,\boldsymbol{X}\boldsymbol{B}_2\right) = 0. \quad (3.19)$$

Since the Riccati equations in (3.9) must typically be solved numerically, we do not propose an analytical procedure for finding actuator and sensor placements yielding $\delta\Gamma_2 = 0$. Instead, we now create a framework where a gradient-based function minimisation can be used to iterate towards the optimal placements. For a set of actuator positions $\{x_a^1, \ldots, x_a^{m_a}\}$ and sensor positions $\{x_s^1, \ldots, x_s^{m_s}\}$, Γ_2 is obtained by solving (3.9) and (3.14). For a perturbation of the jth actuator position x_a^j by an amount δx_a^j, solve (3.16) for $\boldsymbol{\delta X}^j$ and set

$$\frac{\delta\Gamma_2}{\delta x_a^j} = \frac{\mathrm{tr}\left(\boldsymbol{V}^{-1}\boldsymbol{C}_2\boldsymbol{Y}\boldsymbol{\delta X}^j\,\boldsymbol{Y}\boldsymbol{C}_2^*\right)}{\delta x_a^j}. \quad (3.20a)$$

https://doi.org/10.1017/jfm.2011.195 Published online by Cambridge University Press

For a perturbation of the kth sensor position x_s^k by an amount δx_s^k, solve (3.18) for $\delta \boldsymbol{Y}^k$ and set

$$\frac{\delta \Gamma_2}{\delta x_s^k} = \frac{\mathrm{tr}\left(\boldsymbol{R}^{-1}\boldsymbol{B}_2^*\boldsymbol{X}\,\delta\boldsymbol{Y}^k\,\boldsymbol{X}\boldsymbol{B}_2\right)}{\delta x_s^k}. \tag{3.20b}$$

Note that the Riccati solutions $\boldsymbol{X}$ and $\boldsymbol{Y}$ are computed while solving for Γ_2 and can be reused while solving the Lyapunov equations needed for $\nabla\Gamma_2$. Thus, we solve two Riccati equations for every evaluation of Γ_2, and $m_a + m_s$ Lyapunov equations for every evaluation of the $(m_a + m_s)$-by-1 vector $\nabla\Gamma_2$.

This technique for computing $\nabla\Gamma_2$ is similar to the method proposed by Hiramoto *et al.* (2000), but is believed to be more computationally efficient. Because Hiramoto *et al.* computed Γ_2 using the LFT of the controlled system, each component of $\nabla\Gamma_2$ required the solution to a $2N$-by-$2N$ Lyapunov equation; see (3.11)–(3.13). On the other hand, the method we propose reduces this size to N-by-N. Using the Lyapunov equation solvers selected for this study, our proposed method should provide a speedup by a factor of approximately 6.

We employ a Polak-Ribière conjugate gradient method, using a modified Brent's method of line minimisation that uses derivative information. Brent's method also requires a bracketing function that provides bounds on the line minimum. These methods are robust in the sense that they are unlikely to lose numerical stability, and they are generally efficient as well. Implementation details can be found in Press *et al.* (2007).

4. Results

4.1. *Brute force sampling*

To understand the effect of SISO actuator and sensor positions more fully, we first perform a brute force sampling of the LQG-controlled system's H_2 norm. Instead of implementing a minimisation algorithm, we map out $\gamma_2(x_a, x_s)$ over a test matrix spanning actuator and sensor positions in $\{-15.00, -14.75, \ldots, 15.00\}$. The results for a white noise disturbance present across the entire spatial domain are plotted in figure 2(a). In figure 2(b), we run a simulation of the LQG-controlled system and show a sample snapshot. Without control, the state would blow up because the system would be globally unstable.

Some qualitative features are immediately obvious from figure 2(a). First, the optimal placement is approximately $x_a = -1.00$ and $x_s = 1.00$, at which $\gamma_2 = 46.1$; we will refine these numbers later through the use of iterative minimisation. Second, a penalty exists for placing the actuator too far downstream. This is an intuitive result – since the flow in question is convection-driven, a downstream actuator is able to influence less of the physical domain. Third, a similar penalty exists for placing the sensor too far upstream. Recall that the amplification factor $\mu(x)$ is an inverted parabola with roots at ± 8.60. If the sensor is too far upstream, then the detected disturbances naturally dampen before they reach the region of amplification. Thus, the disturbances amplified in this region would not primarily be the ones observed by the sensor. Finally, excessive time lag (positioning the sensor too far downstream of the actuator) has a detrimental effect on perturbation control. This is also a result of the convection-driven nature of the system. If the sensor is too far downstream of the actuator, then the information it receives will have already passed the actuator for some time. Thus, the actuator would be acting on outdated information, and the feedback would effectively result in a time lag.

https://doi.org/10.1017/jfm.2011.195 Published online by Cambridge University Press

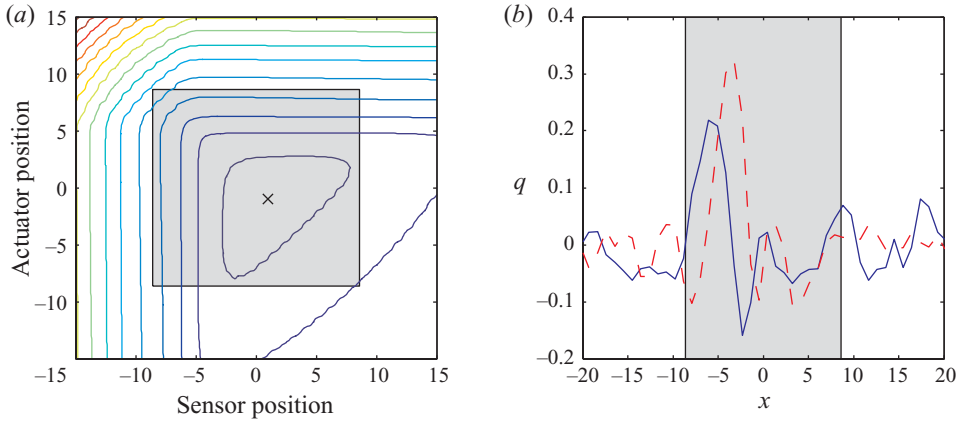


FIGURE 2. (Colour online available at journals.cambridge.org/FLM) (*a*) Contours of $\log_{10}\gamma_2$ and the optimal placement ($\times$), with disturbances introduced everywhere. The innermost contour is $\log_{10}\gamma_2 = 2$, and each subsequent contour increments by 0.5. (*b*) A sample snapshot of the controlled perturbation q, shown as real (solid/blue) and imaginary (dashed/red) parts. The actuator is at $x_a = -1.00$ and the sensor is at $x_s = 1.00$. In both plots, the region of amplification is shaded grey.

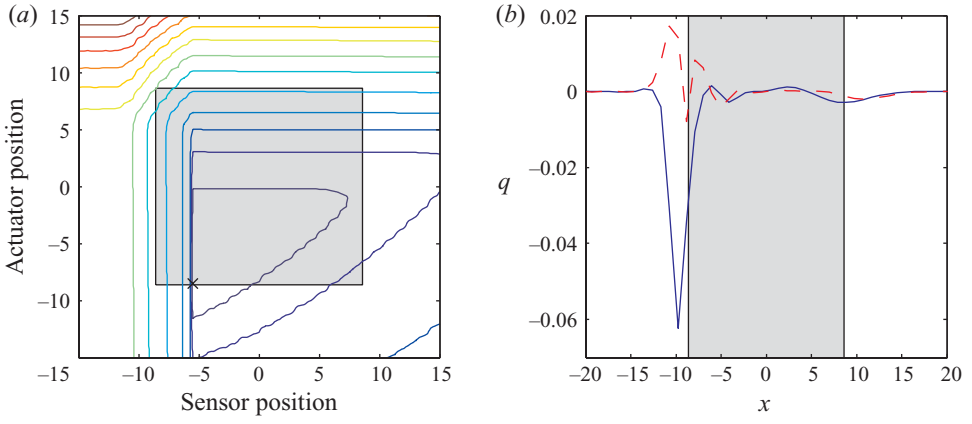


FIGURE 3. (Colour online) (*a*) Contours of $\log_{10}\gamma_2$ and the optimal placement ($\times$), for the case of an upstream disturbance introduced at $x_d = -11.00$. The innermost contour is $\log_{10}\gamma_2 = 1.0$, and each subsequent contour increments by 0.5. (*b*) A sample snapshot of the controlled perturbation q, shown as real (solid/blue) and imaginary (dashed/red) parts. The actuator is at $x_a = -8.50$ and the sensor is at $x_s = -5.50$. In both plots, the region of amplification is shaded grey.

Data for a flow disturbance introduced around $x_d = -11.00$ are shown in figure 3(*a*), with a sample snapshot shown in figure 3(*b*). The qualitative features of this $\gamma_2(x_a, x_s)$ map are similar to those of figure 2(*a*), but we highlight a few differences. First, the optimal placement is now approximately $x_a = -8.50$ and $x_s = -5.50$, which is much further upstream than in the previous case. In the sample snapshot shown in figure 3(*b*), we note that the controller is extremely effective in reducing the perturbation magnitude within the region of amplification.

Intuitively, we might expect an optimal placement $x_s \approx x_d$, so that the sensor placement coincides with the disturbance source. Indeed, such a placement allows

https://doi.org/10.1017/jfm.2011.195 Published online by Cambridge University Press

the state estimate $\hat{\boldsymbol{q}}$ to match the true state $\boldsymbol{q}$ very closely in the disturbance region. This placement, however, is far from optimal. As a result of the strong amplification downstream of the disturbance source, even the smallest estimator error $\boldsymbol{e} = \hat{\boldsymbol{q}} - \boldsymbol{q}$ in the disturbance region can amplify significantly. By placing the sensor downstream of the disturbance source, the estimator is better able to reduce the error $\boldsymbol{e}$ in the region of amplification, where accurate state estimation is critically important.

The second difference in the case of upstream disturbances is that the optimal placement is not robust. Although the optimal placement is unique, figure 3(*a*) shows that a small upstream shift in x_s drastically increases γ_2. The topography of the $\gamma_2(x_a, x_s)$ function contains a cliff near $x_s = -5.50$ where the H_2 norm increases suddenly. Holding $x_a = -8.50$ but moving $x_s = -5.50$ to -5.75, the H_2 norm γ_2 increases from 3.87 to 138. This occurs because the shift in the sensor location causes a small zero of the $\boldsymbol{u}$-to-$\boldsymbol{y}$ transfer function to move from the left-half-plane to the right-half-plane. When this occurs, the small right-half-plane zero introduces significant bandwidth limitations for disturbance rejection. A sensitivity function analysis indicates considerably inferior disturbance rejection at frequencies $\omega < 10$.

This non-robustness appears to indicate the importance of placing the sensor firmly within the region of high amplification, lest estimator errors grow beyond acceptable limits. For instance, in an actual two- or three-dimensional flow setup without *a priori* knowledge of the optimal sensor placement, an experimenter could guess a sensor placement where amplification is expected. (Recall that the dynamics of fluid systems are often strongly non-normal (Chomaz 2005), so regions of transient amplification may not correspond well with unstable eigenmodes of the linearised dynamics.)

Besides these two major differences, the general form of the γ_2 solution is similar to the case where disturbances are present everywhere. Level sets of γ_2 have a near-triangular form, with penalties on placing the actuator too far downstream, placing the sensor too far upstream, and creating excessive separation between sensors and actuators. The general similarities between figures 2(*a*) and 3(*a*) indicate that it is possible to find an actuator and sensor placement that is effective for both disturbance types. For example, if $x_a = -3.50$ and $x_s = 0.00$, then $\gamma_2 = 53.6$ when disturbances are present everywhere and $\gamma_2 = 5.90$ when disturbances are concentrated upstream. These are acceptably close to the respective optimal values of 46.1 and 3.86. If other disturbance types retain the same qualitative nature of $\gamma_2(x_a, x_s)$, then a 'universally' optimal placement could feasibly be sought.

We also perform brute force sampling for the two-actuator, two-sensor configuration with disturbances present everywhere. The placement is optimal at about $x_a = -3.75, 2.75$ and $x_s = -2.75, 3.75$, for which $\gamma_2 = 34.0$. (Results are not plotted here.) As in the SISO case, these numbers are not precise, and are later refined using an iterative procedure. One common feature in MIMO results is that if one actuator or sensor is placed near the optimal position, then the effect of the other actuator or sensor placement on γ_2 is generally not large.

4.2. *Conjugate gradient minimisation*

The optimal placement for different numbers of actuators and sensors, as found using conjugate gradient minimisation, is shown in figure 4(*a*) for disturbances present everywhere. The iterative method more accurately puts the optimal SISO placement at $x_a = -1.03$, $x_s = 0.98$ and the optimal two-actuator, two-sensor placement at $x_a = -3.78, 2.71$, $x_s = -2.75, 3.74$. An approximate symmetry around $x = 0$ between actuator and sensor placement is apparent. Additionally, a simple pattern exists for configurations with an equal number of actuators and sensors. The optimal placement

https://doi.org/10.1017/jfm.2011.195 Published online by Cambridge University Press

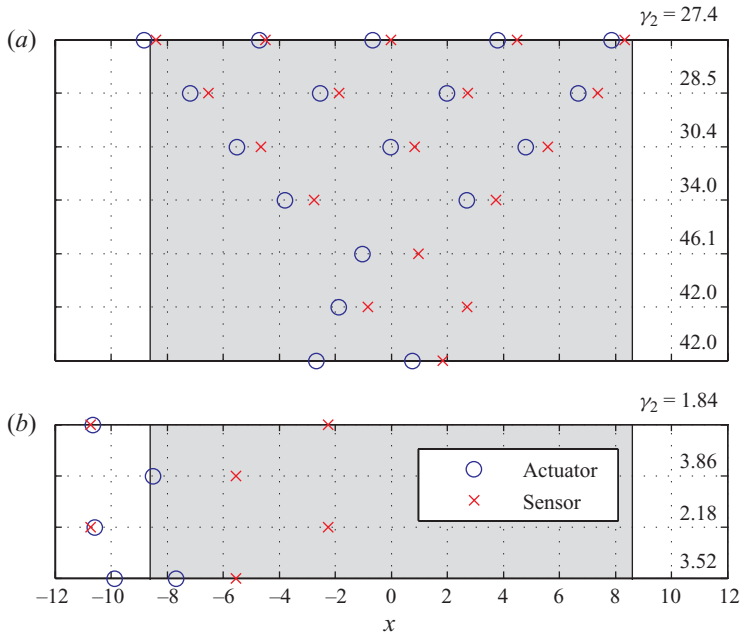


FIGURE 4. (Colour online) Each row shows the optimal placement for some number of actuators and sensors. The H_2 norm γ_2 is tabulated for each configuration, and the region of amplification is shaded grey. (*a*) Disturbances present everywhere. (*b*) Disturbances introduced at $x_d = -11.0$. The first row is the optimal placement for two actuators and two sensors; the actuators are collocated.

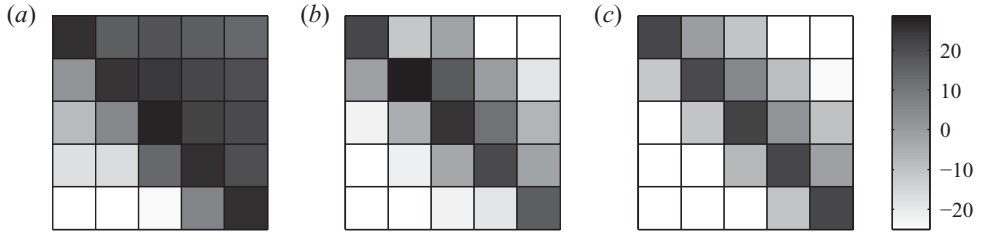


FIGURE 5. The LQG gain in the optimally placed five-input, five-output system, shown in decibels. The block in row j and column k shows the gain from a signal $\exp(\mathrm{i}\omega t)$ in sensor k to actuator j, assuming that the sensors and actuators are ordered from upstream to downstream. (*a*) At $\omega = 10^{-1}$; (*b*) at $\omega = 10^{1}$ and (*c*) at $\omega = 10^{3}$.

favors near-collocation of actuator and sensor pairs, with each actuator placed slightly upstream of each sensor. This allows the sensors to measure the effect of the actuators without a large time lag. As the number of actuators and sensors increases, the actuator–sensor pairs spread out across the spatial domain, and the spacing within pairs becomes tighter. Figure 4(*a*) shows that the placement of the pairs forms an orderly geometric pattern as the number of pairs increases.

A transfer function analysis of the controller gain $\boldsymbol{K}$ from $\boldsymbol{y}$ to $\boldsymbol{u}$ shows that the communication between sensors and actuators primarily occurs within pairs, especially at higher frequencies. (See (3.10) for the formulation of $\boldsymbol{K}$.) This is illustrated in figure 5, which supposes the optimally placed five-input, five-output system shown in the top row of figure 4(*a*). These three plots show the LQG gain from each sensor to each actuator, given that each sensor receives a signal $\exp(\mathrm{i}\omega t)$. At lower

https://doi.org/10.1017/jfm.2011.195 Published online by Cambridge University Press

frequencies (figure 5*a*), the gain from downstream sensors to upstream actuators is still non-trivial. This feedback aids the performance of the upstream actuators. At higher frequencies, the primarily diagonal structure of the gain matrices indicates that communication outside the pairs is weak. The diffusive nature of the Ginzburg–Landau operator dampens high frequency oscillations, so such oscillations do not propagate effectively across large distances. Therefore, high-frequency control is most effective within actuator–sensor pairs.

The optimal placements in the case of upstream disturbances are illustrated in figure 4(*b*). For the limited number of configurations tested, the optimal actuator and sensor placements are upstream of the origin. In SISO control, the optimal placement is $x_a = -8.48$ and $x_s = -5.55$. When employing one actuator and two sensors, the cost γ_2 is very insensitive to the precise placement of the downstream sensor. Moving that sensor's location anywhere from $x = -5$ to 15 changes γ_2 by not more than 0.04%. Nevertheless, the combination of the upstream sensor near the disturbance source and the downstream sensor far in the wake allows for very accurate estimation in the entire domain of interest. The optimal two-actuator, two-sensor placement collocates the actuators and roughly reproduces the one-actuator, two-sensor placement. The fact that both actuators are optimally placed near the disturbance source suggests that no other actuator location can be as effective. Finally, we remark that the optimal two-actuator, one-sensor configuration is like the optimal SISO configuration, but it is possible to actuate near the disturbance source without causing serious time delays.

For each actuator–sensor configuration, figure 4 also tabulates the H_2 norm γ_2 from the disturbances to the perturbation and input costs. As expected, γ_2 decreases as the number of actuators and sensors increases. This simply indicates that the control objective is easier to attain when more actuators and sensors are available. In figure 4(*a*), however, the decrease in γ_2 tapers off when increasing the number of actuator–sensor pairs from one to five. Furthermore, in figure 4(*b*), the improvement to the base SISO case by adding one actuator is not as great as the improvement by adding one sensor. In choosing the number of actuators and sensors to use, an experimenter should consider a tradeoff between how much the perturbation and input need to be minimised, and how many actuators and sensors can be afforded. Other factors, such as the way disturbances are introduced, also affect this decision. We may observe, for instance, that the multiplicative reduction in γ_2 from SISO to two-input, two-output control is more significant in figure 4(*b*) than in figure 4(*a*).

4.3. *Further remarks*

When performing an iterative technique, it is important to note the computational effort required. The linearised Ginzburg–Landau system presented here is accurately represented using only 100 states; however, iterating on higher-dimensional systems may be intractable if a large number of function calls is required. A complete discussion on the computational effort required to minimise Γ_2 is beyond the scope of this paper. The effort would heavily depend on the choice of a minimisation algorithm, its numerical tolerances and the initial conditions chosen.

As previously mentioned, each evaluation of Γ_2 requires solving two N-by-N Riccati equations (3.9), and each evaluation of $\nabla\Gamma_2$ requires solving $m_a + m_s$ N-by-N Lyapunov equations (3.16) and (3.18). The bracketing function additionally requires a number of N-by-N Riccati solutions that is generally *a priori* unknown. With the algorithms chosen, scaling experiments show that for $40 \leqslant N \leqslant 200$, the CPU times of one Riccati solution and one Lyapunov solution both scale by about $N^{2.5}$. On a 2.66 GHz dual-core Core i7-620M processor, each Riccati solution requires about

https://doi.org/10.1017/jfm.2011.195 Published online by Cambridge University Press

	SISO				Two-actuator, two-sensor					
					x_a		x_s			
β	x_a	x_s	γ_q/β	γ_u					γ_q/β	γ_u
1	−1.39	0.04	7.14	4.15	−3.25	3.17	−2.77	2.86	5.23	3.24
3	−1.02	0.92	6.59	6.33	−3.72	2.57	−2.79	3.65	4.86	4.69
7	−1.03	0.98	6.48	8.22	−3.78	2.71	−2.75	3.74	4.77	6.20
15	−1.04	1.01	6.44	11.1	−3.79	2.70	−2.73	3.77	4.74	8.30
50	−1.04	1.03	6.42	19.0	−3.80	2.70	−2.71	3.79	4.72	14.3

TABLE 2. Optimal placement, perturbation size and input size for different β, with disturbances present everywhere.

150 ms for $N = 100$, and each Lyapunov equation requires about 59 ms. The total number of equations to be solved depends heavily on the $\gamma_2(\{x_a\}, \{x_s\})$ topography and the choice of tolerances and initial conditions. It suffices to state that the CPU time for convergence increases significantly as the number of actuators and sensors increases.

For the results presented in this study, the $\gamma_2(\{x_a\}, \{x_s\})$ function topography is relatively simple. Global minima can be found by guessing multiple initial conditions and checking for common convergence. Performing a coarse brute force search also aids in picking good initial conditions. Beyond these simple configurations, however, convergence to a global minimum can be difficult. This is especially true when disturbances are only introduced upstream, or when unequal numbers of actuators and sensors are used. Good initial conditions are particularly important in these cases. Bad initial conditions may cause the iterator to converge very slowly, quit prematurely or fail to converge to the global minimum. A global minimisation technique, such as simulated annealing, would then be necessary to ensure that a local minimum found is indeed the absolute minimum.

The choice of cost matrices also affects the computed optimal placement. As aforementioned, the vector costs used are $\boldsymbol{J}_1 = \boldsymbol{Q}^{1/2}\boldsymbol{q}$ and $\boldsymbol{J}_2 = \boldsymbol{R}^{1/2}\boldsymbol{u}$, where $\boldsymbol{Q}^{1/2} = \beta \boldsymbol{M}^{1/2}$ and $\boldsymbol{R}^{1/2} = \boldsymbol{I}$. The positive scalar β controls the balance between minimising $\boldsymbol{q}$ and minimising $\boldsymbol{u}$. To quantify their sizes individually, let γ_q be the H_2 norm of the transfer function from $\boldsymbol{w}$ to $\boldsymbol{J}_1$, and let γ_u be the H_2 norm of the transfer function from $\boldsymbol{w}$ to $\boldsymbol{J}_2$. These are calculated using the LFT formulation (3.11) by, respectively, setting $\boldsymbol{Z_C} = \begin{bmatrix}\boldsymbol{C}_1 & 0\end{bmatrix}$ and $\boldsymbol{Z_C} = \begin{bmatrix}0 & -\boldsymbol{D}_{12}\boldsymbol{F}\end{bmatrix}$, and computing $\sqrt{\Gamma_2}$ by (3.12) and (3.13). It can be shown that $\gamma_q^2 + \gamma_u^2 = \gamma_2^2$. A measure of the perturbation size is then given by γ_q/β and the input size by γ_u. For different choices of β, optimal positions and corresponding values of γ_q/β and γ_u are listed in table 2. (Note that the optimal controller and positions depend not on $\boldsymbol{Q}$ and $\boldsymbol{R}$ individually, but rather only β.)

We immediately see that within a fairly large range of β, the optimal actuator and sensor placement is robust to the exact choice of β. This is consistent with findings by Lauga & Bewley (2003). As expected, a larger β is more effective at reducing the perturbation magnitude, but at a greater input expense. In practice, one would choose β based on this tradeoff. We select $\beta = 7$ because it maintains a small perturbation magnitude using reasonably sized inputs. Lauga & Bewley (2004) discusses the effect of β on the Ginzburg–Landau system's closed loop eigenvalues.

We also remark briefly that the controller designed from the linearised model is effective in the full, nonlinear Ginzburg–Landau model. The cubic term in (2.1)

https://doi.org/10.1017/jfm.2011.195 Published online by Cambridge University Press

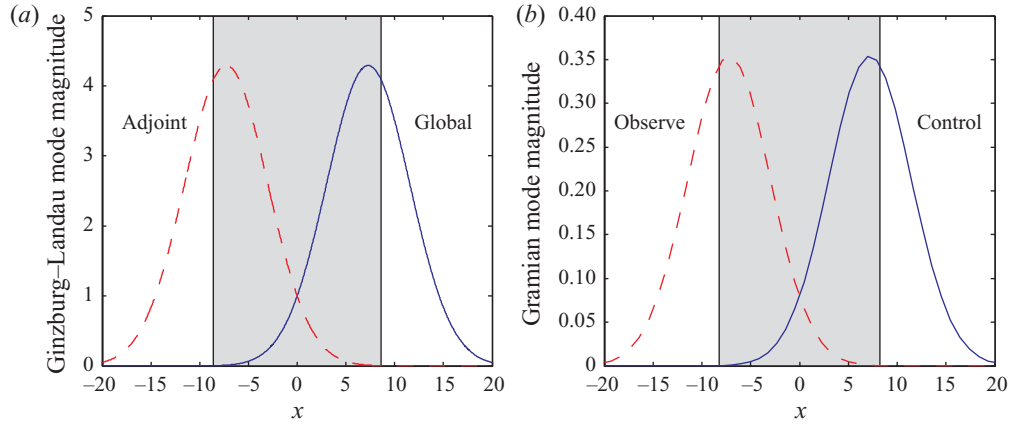


FIGURE 6. (Colour online) (*a*) Leading global and adjoint eigenmode magnitudes, for $\mu_0 = 1.03\mu_c$. (*b*) Leading modes of the observability and controllability Gramians (assuming full sensing and actuation), for $\mu_0 = 0.96\mu_c$. The region of amplification is shaded grey.

always drives the state q towards zero, aiding the controller in doing the same. Brief numerical experiments show, however, that the optimal placement in the nonlinear model does not necessarily correspond with that of the linear model. Further study is necessary to establish optimal placement in that case.

5. Comparison with previous approaches

We might naively believe that the optimal actuator and sensor placement could be determined directly from a global mode analysis. In this analysis, we would place sensors where the most unstable eigenmodes are large, so that growing disturbances would register a large output. Similarly, we would place actuators where the most unstable adjoint eigenmodes are large. This is supported by the fact that the LQG controller's construction requires plant detectability and stabilisability (Doyle *et al.* 1989). Bagheri *et al.* (2009) and Åkervik *et al.* (2007) used this approach for actuator and sensor placement. While this method is plausible on intuitive grounds, it does not produce optimal results. With global and adjoint modes given by (2.3), we find for $\mu_0 = 1.03\mu_c$ that there is one unstable mode and one unstable adjoint mode (Bagheri *et al.* 2009). These two mode magnitudes are bell curves, with peaks, respectively, at $x = 7.28$ and $x = -7.28$ (see figure 6*a*). If flow disturbances were introduced everywhere, and a sensor and actuator were placed at these two points, then (3.14) would yield $\gamma_2 = 259$. This is far from the optimal $\gamma_2 = 46.1$ achieved by placing the actuator at $x_a = -1.03$ and the sensor at $x_s = 0.98$.

The global mode analysis fails to reveal the optimal placement because the linearised Ginzburg–Landau operator is strongly non-normal. In general, the non-normality prevents global mode analysis from accurately predicting transient growth (Bagheri *et al.* 2009). In this system, as in Navier–Stokes systems, the disturbances that cause large transient growth are known not to correspond well with the most unstable eigenmodes (Trefethen *et al.* 1993). In principle, one may be able to circumvent this issue in a stable system by placing an actuator where an optimal harmonic forcing causes the greatest steady-state solution. The optimal harmonic forcing in the adjoint system could also yield a sensor placement. Bagheri *et al.* (2009) performed a related

https://doi.org/10.1017/jfm.2011.195 Published online by Cambridge University Press

analysis in which the initial condition leading to the largest transient growth was sought. The magnitude of this optimal initial condition was a bell curve centred near the upstream boundary of the amplification region, and therefore would not yield the optimal actuator location. Consult Trefethen *et al.* (1993) and Schmid & Henningson (2000) for more details.

A similar analysis could be done using controllability and observability Gramians of the uncontrolled system with full sensing and actuation. This system is governed by $(\boldsymbol{A}, \boldsymbol{B}, \boldsymbol{C})$ representing

$$\dot{\boldsymbol{q}} = \boldsymbol{A}\boldsymbol{q} + \boldsymbol{B}\boldsymbol{d} \tag{5.1a}$$

$$\boldsymbol{y} = \boldsymbol{C}\boldsymbol{q}, \tag{5.1b}$$

where $\boldsymbol{B} = \boldsymbol{I}$ and $\boldsymbol{C} = \boldsymbol{M}$. The adjoint system is governed by $(\boldsymbol{A}^+, \boldsymbol{C}^+, \boldsymbol{B}^+)$. Because of the uneven grid spacing, the adjoint is not the same as the complex conjugate (Bagheri *et al.* 2009); rather,

$$\boldsymbol{A}^+ = \boldsymbol{M}^{-1}\boldsymbol{A}^*\boldsymbol{M} \tag{5.2a}$$

$$\boldsymbol{B}^+ = \boldsymbol{B}^*\boldsymbol{M} \tag{5.2b}$$

$$\boldsymbol{C}^+ = \boldsymbol{M}^{-1}\boldsymbol{C}^*. \tag{5.2c}$$

The controllability Gramian $\boldsymbol{W}_c$ and the observability Gramian $\boldsymbol{W}_o$ are the solutions to the Lyapunov equations

$$\boldsymbol{A}\boldsymbol{W}_c + \boldsymbol{W}_c\boldsymbol{A}^+ + \boldsymbol{B}\boldsymbol{B}^+ = 0 \tag{5.3a}$$

$$\boldsymbol{A}^+\boldsymbol{W}_o + \boldsymbol{W}_o\boldsymbol{A} + \boldsymbol{C}^+\boldsymbol{C} = 0. \tag{5.3b}$$

In this analysis, we expect the leading eigenvector of $\boldsymbol{W}_c$ to be large where the state is sensitive to the disturbance $\boldsymbol{d}$; this would appear to be a good place to put a sensor. Similarly, we expect the leading eigenvector of $\boldsymbol{W}_o$ to be large where the uncontrolled dynamics are most sensitive to perturbations; this would appear to be a good place to put an actuator. These eigenvectors are shown in figure 6(b) with $\mu_0 = 0.96\mu_c$, since Gramians are only well defined for globally stable systems.

Once again, we find that this analysis does not correctly predict the optimal SISO placement. For this subcritical Ginzburg–Landau system, the optimal placement is $x_a = -0.98$ and $x_s = 0.95$, yielding $\gamma_2 = 42.8$. The Gramian analysis, on the other hand, predicts $x_a = -7.0$ and $x_s = 7.0$, yielding $\gamma_2 = 188$. This analysis fails because Gramians, by construction, decouple actuation from sensing. This is apparent from (5.3). When actuation and sensing are decoupled, the convective nature of information propagation is completely ignored. Placing the sensor so far downstream of the actuator effectively introduces a large time lag in the feedback control.

A method proposed by Giannetti & Luchini (2007) yields a better estimate of the optimal actuator and sensor placement when disturbances are present everywhere. Giannetti & Luchini define the 'wavemaker' region as the part of the domain where

$$\zeta(x) = \frac{\phi_0(x)\,\bar{\psi}_0(x)}{\langle \phi_0, \psi_0 \rangle} \tag{5.4}$$

has a large magnitude, given a global mode ϕ_0 and adjoint mode ψ_0; see (2.3). They employed a perturbation technique to show that in this wavemaker region, a change in $\boldsymbol{A}$ creates the largest possible change in the corresponding eigenvalue λ_0. As a validation of their theory, Giannetti & Luchini showed good agreement between the

https://doi.org/10.1017/jfm.2011.195 Published online by Cambridge University Press

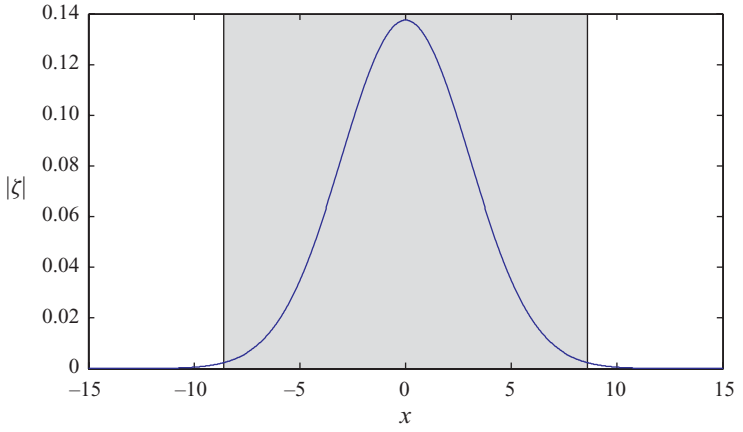


FIGURE 7. (Colour online) The global and adjoint mode overlap $|\zeta(x)|$ for the unstable mode. The region of amplification is shaded grey.

wavemaker region of the unstable cylinder wake and the effective placement of passive actuation in Strykowski & Sreenivasan (1990). Although we do not seek to change $\boldsymbol{A}$, the wavemaker region nevertheless indicates a region of high dynamical sensitivity (Chomaz 2005). In such a region, an actuator has a powerful influence on the flow, and localised feedback is effective. Lauga & Bewley (2004) used the wavemaker to determine their actuator and sensor placement and reported effective H_∞ control.

As shown in figure 7, the unstable global mode has the largest overlap with its corresponding adjoint mode at $x = 0$ when $\mu_0 = 1.03\mu_c$. Therefore, we propose that placing actuators and sensors near the origin is a sensible initial condition for iterative function minimisation. Although this is a crude approximation for optimal placement, it remains more accurate than global mode and Gramian analyses.

6. Conclusion

The linearised Ginzburg–Landau equation is a simple model describing the temporal and spatial evolution of small flow perturbations. In this paper, we control the linearised Ginzburg–Landau equation by establishing a standard LTI state space with some number of actuators and sensors. We perform a perturbation analysis on the continuous algebraic Riccati equations that determine the H_2 optimal controller. From this, we derive a formulation for the gradient of the controlled system's H_2 squared norm. This formulation, which is similar to but more efficient than the formulation of Hiramoto *et al.* (2000), is applicable to any LQG-controlled system where actuation and sensing matrices are to be optimised. We use conjugate gradient function minimisation to iterate towards the linearised Ginzburg–Landau system's optimal actuator and sensor placement. This is but one example of how the perturbation theory can be used.

The conjugate gradient results agree with brute force mappings of the H_2 norm over a large domain. When one actuator and sensor are available and flow disturbances are introduced everywhere, the optimal placement is $x_a = -1.03$ and $x_s = 0.98$ for the LQG cost matrices chosen. The brute force mappings show that there exist penalties for placing the actuator too far downstream, the sensor too far upstream, or the actuator too far upstream of the sensor. When an equal number of actuators and sensors is employed, it is optimal to place actuators and sensors in distinct pairs. Each actuator

https://doi.org/10.1017/jfm.2011.195 Published online by Cambridge University Press

is slightly upstream of the corresponding sensor, and pairs are distributed throughout the region of amplification. We show that the optimal placement is relatively robust to the precise scaling of cost matrices.

When the disturbance is centred at $x_d = -11.0$, the optimal placement is $x_a = -8.48$ and $x_s = -5.55$. Optimal MIMO placements are upstream of the origin, but no clear patterns emerge. Regardless of the way disturbances are introduced, the control system's performance increases by adding more actuators and sensors, but the increase may not be significant. When optimising the control performance in an experimental set-up, for instance, a greater improvement may be achieved by tuning the existing actuator and sensor placements than by simply adding more actuators and sensors.

The process of finding the optimal placement in the linearised Ginzburg–Landau system is completely tractable on a modern computer. Convergence to the global optimum can be difficult, however, when an unequal number of actuators and sensors is used, or when the flow disturbances are only introduced upstream.

Although global mode and Gramian analyses are standard techniques in LTI systems, neither is able to reproduce the optimal actuator and sensor placement. Both roughly suggest $x_a = -7$ and $x_s = 7$, yielding an H_2 norm four to six times larger than the true minimum when disturbances are present everywhere. The global mode analysis fails because the underlying dynamics are strongly non-normal, and the Gramian analysis fails because it inherently decouples actuation from sensing. On the other hand, we propose that wavemaker analysis is a better way to seek the optimal placement. Although it does not immediately yield the optimal placement, it provides a sensible guess of $x_a = x_s = 0.0$. This is a good initial condition for iterative minimisation.

The methods and results presented may be extended to two- or three-dimensional flow control problems. In such cases, the state size would likely be so large that Riccati and Lyapunov solutions would be computationally intractable. Therefore, each evaluation of the H_2 norm and its gradient would likely require the construction of a reduced-order model, for instance using balanced proper orthogonal decomposition or the eigensystem realisation algorithm (Ma, Ahuja & Rowley 2011). Alternatively, iterative methods that bypass the model reduction process may be preferred (Luchini & Bewley 2010). Potentially faster minimisation algorithms, such as quasi-Newton iteration, may also be substituted (Press *et al.* 2007). We posit that with such techniques, optimisation of actuator and sensor placement in Navier–Stokes systems should remain computationally tractable using high-performance computing.

This work was supported by the National Science Foundation, grant CMMI-0932928, and K.C. received support from the United States Department of Defense (DOD) through the National Defense Science & Engineering Graduate (NDSEG) Fellowship Program. We thank Professor Tim Colonius, Professor Paolo Luchini, Professor Shervin Bagheri, and Miloš Ilak for guidance and advising.

REFERENCES

Åkervik, E., Hœpffner, J., Ehrenstein, U. & Henningson, D. S. 2007 Optimal growth, model reduction and control in a separated boundary-layer flow using global eigenmodes. *J. Fluid Mech.* **579**, 305–314.

Bagheri, S., Henningson, D. S., Hœpffner, J. & Schmid, P. J. 2009 Input-output analysis and control design applied to a linear model of spatially developing flows. *Appl. Mech. Rev.* **62** (2), 020803.

https://doi.org/10.1017/jfm.2011.195 Published online by Cambridge University Press

Chomaz, J.-M. 2005 Global instabilities in spatially developing flows: non-normality and nonlinearity. *Annu. Rev. Fluid Mech.* **37**, 357–392.

Chomaz, J.-M., Huerre, P. & Redekopp, L. G. 1988 Bifurcations to local and global modes in spatially developing flows. *Phys. Rev. Lett.* **60** (1), 25–28.

Cossu, C. & Chomaz, J.-M. 1997 Global measures of local convective instabilities. *Phys. Rev. Lett.* **78** (23), 4387–4390.

Doyle, J. C., Glover, K., Khargonekar, P. P. & Francis, B. A. 1989 State-space solutions to standard H_2 and H_∞ control problems. *IEEE Trans. Autom. Control* **34** (8), 831–847.

Giannetti, F. & Luchini, P. 2007 Structural sensitivity of the first instability of the cylinder wake. *J. Fluid Mech.* **581**, 167–197.

Gillies, E. A. 2001 Multiple sensor control of vortex shedding. *AIAA J.* **39** (4), 748–750.

Halim, D. & Moheimani, S. O. R. 2003 An optimization approach to optimal placement of collocated piezoelectric actuators and sensors on a thin plate. *Mechatronics* **13** (1), 27–47.

Hiramoto, K., Doki, H. & Obinata, G. 2000 Optimal sensor/actuator placement for active vibration control using explicit solution of algebraic Riccati equation. *J. Sound Vib.* **229** (5), 1057–1075.

Huerre, P. & Monkewitz, P. A. 1990 Local and global instabilities in spatially developing flows. *Annu. Rev. Fluid Mech.* **22**, 473–537.

Kim, J. & Bewley, T. R. 2007 A linear systems approach to flow control. *Annu. Rev. Fluid Mech.* **39**, 383–417.

Kondoh, S., Yatomi, C. & Inoue, K. 1990 The positioning of sensors and actuators in the vibration control of flexible systems. *JSME Intl J. Ser.* III **33** (2), 145–152.

Lauga, E. & Bewley, T. R. 2003 The decay of stabilizability with Reynolds number in a linear model of spatially developing flows. *Proc. R. Soc.* A **459** (2036), 2077–2095.

Lauga, E. & Bewley, T. R. 2004 Performance of a linear robust control strategy on a nonlinear model of spatially developing flows. *J. Fluid Mech.* **512**, 343–374.

Luchini, P. & Bewley, T. R. 2010 Methods for the solution of very large flow-control problems that bypass open-loop model reduction. In *Sixty-third Annual Meeting of the APS Division of Fluid Dynamics*. American Physical Society, Long Beach, CA, USA.

Ma, Z., Ahuja, S. & Rowley, C. W. 2011 Reduced-order models for control of fluids using the eigensystem realization algorithm. *Theor. Comput. Fluid Dyn.* **25** (1–4), 233–247.

Moheimani, S. O. R. & Ryall, T. 1999 Considerations on placement of piezoceramic actuators that are used in structural vibration control. In *Proc. 38th Conference on Decision & Control*, pp. 1118–1123. IEEE.

Press, W. H., Teukolsky, S. A., Vetterling, W. T. & Flannery, B. P. 2007 *Numerical Recipes*, 3rd edn. Cambridge University Press.

Roussopoulos, K. 1993 Feedback control of vortex shedding at low Reynolds numbers. *J. Fluid Mech.* **248**, 267–296.

Roussopoulos, K. & Monkewitz, P. A. 1996 Nonlinear modelling of vortex shedding control in cylinder wakes. *Physica* D **97** (1–3), 264–273.

Schmid, P. J. 2007 Nonmodal stability theory. *Annu. Rev. Fluid Mech.* **39**, 129–162.

Schmid, P. J. & Henningson, D. S. 2000 *Stability and Transition in Shear Flows*. Springer.

Skogestad, S. & Postlethwaite, I. 2005 *Multivariable Feedback Control: Analysis and Design*, 2nd edn. John Wiley & Sons Ltd.

Sreenivasan, K. R., Strykowski, P. J. & Olinger, D. J. 1987 Hopf bifurcation, Landau equation, and vortex shedding behind circular cylinders. In *Proc. Forum on Unsteady Flow Separation* (ed. K. N. Ghia), pp. 1–13. ASME.

Strykowski, P. J. & Sreenivasan, K. R. 1990 On the formation and suppression of vortex 'shedding' at low reynolds numbers. *J. Fluid Mech.* **218**, 71–107.

Trefethen, L. N., Trefethen, A. E., Reddy, S. C. & Driscoll, T. A. 1993 Hydrodynamic stability without eigenvalues. *Science* **261** (5121), 578–584.

Weideman, J. A. C. & Reddy, S. C. 2000 A MATLAB differentiation matrix suite. *ACM Trans. Math. Softw.* **26** (4), 465–519.

Williamson, C. H. K. 1996 Vortex dynamics in the cylinder wake. *Annu. Rev. Fluid Mech.* **28**, 477–539.

https://doi.org/10.1017/jfm.2011.195 Published online by Cambridge University Press